ASYMMETRY REDUCTION IN DOUBLE EAGLE +

Myron J. Mandell
Andrew Wilson

S-CUBED
P. O. Box 1620
La Jolla, CA 92038

1. Introduction

Asynchronism in the arrival of power at the insulator-vacuum interface of a pulsed power machine leads directly to a loss of power delivered to that interface[1], in addition to problems associated with possible loss of insulation. With the advent of larger pulsed power machines composed of multiple modules feeding a central vacuum region, the need to reduce the asymmetry in the power density delivered to that region has become an issue of some importance. The asymmetry might result from switching in the individual modules or, as we discuss here, from geometrical effects. In this paper we examine how such geometrical asymmetries in Double EAGLE[2] might be mitigated.

The Double EAGLE pulsed power machine[2] at Physics International consists of two transmission lines which feed power to a common load. Converting from two lines to a central axisymmetric load leads to asymmetries in the power flux density around the periphery of the load, as is shown schematically below.

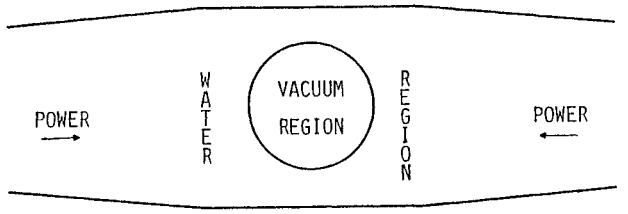

Figure 1. Schematic View of Double EAGLE Coupler Region.

Consider two planar strip transmission lines connected to a circular load. The power pulse will arrive at the power-facing points of the arc (left-right) significantly earlier than at the top-bottom points. The non-simultaneity of arrival at different points on the load (of radius R) gives rise to non-uniformity in the voltage circuit and hence power.

To circumvent this problem a Transit Time Equalizer (TTE) has been devised to increase the path length for signals moving near the center of the strip-line. It consists of a hump whose dimensions are chosen to add a delay time $\tau = R/c$ to signals propagating over it. An artist's impression of the TTE in the region where coupling of the linear transmission lines to the central load takes place is shown in Figure 2.

2. Theoretical Model

We have studied computationally the propagation of power in this coupler. Clearly the geometry is quite complex. To simplify matters we have examined only the propagation of signals which have characteristic wavelengths, $\lambda = ct_0$ (where t_0 is the characteristic pulse time and c the signal speed) which are long compared to the distance Δ between the opposing conducting surfaces. Under this simplification the electric field E is constant across the gap or, more correctly, along a curve that intersects normally opposite surfaces. We need consider then only the normal component of the E-field, E, and may ignore all variations in the normal direction. We work in terms of the vector potential, $\tilde{A}$, given by

$$\vec{E} = -\frac{\partial \tilde{A}}{\partial t} \tag{1}$$

$$\vec{B} = \nabla \times \vec{A} \tag{2}$$

$$\nabla \cdot \vec{A} = 0 \tag{3}$$

From Maxwell's equations

$$\frac{\partial^2 \vec{A}}{\partial t^2} = -c^2 \vec{\nabla} \times \vec{\nabla} \times \vec{A} = c^2 \nabla^2 \vec{A} \tag{4}$$

Equation 4 is strictly valid for a vacuum line or, if we replace E by $D = \varepsilon E$, for a line with a constant dielectric ε such that $c = c_0 \varepsilon^{-1/2}$ where c_0 is the velocity of light in vacuum.

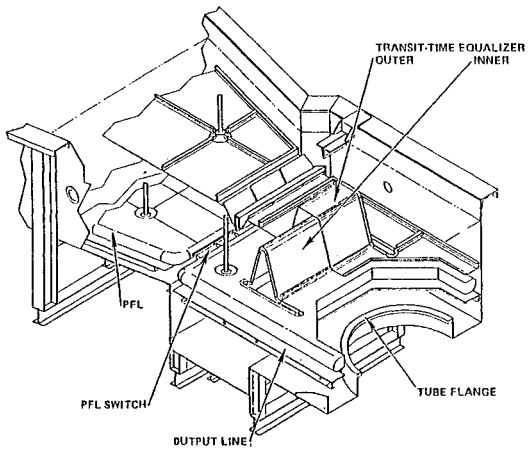

Figure 2. PFL and Coupler Regions.

To solve this equation we use the usual leap-frog algorithm. What is more important is how the discretization of this equation is performed. Briefly the computational mesh shown in Figure 3 is broken into a set of volume elements. Assuming a bilinear variation of the field quantities E,A over these finite elements, the operator ∇^2 can be constructed using the finite element method. The finite element formulation is described in the appendix.

+ Work Supported by DNA

Report Documentation Page

Form Approved
OMB No. 0704-0188

1. REPORT DATE	2. REPORT TYPE	3. DATES COVERED
JUN 1983	**N/A**	**-**

4. TITLE AND SUBTITLE	5a. CONTRACT NUMBER
Asymmetry Reduction In Double Eagle	5b. GRANT NUMBER
	5c. PROGRAM ELEMENT NUMBER
6. AUTHOR(S)	5d. PROJECT NUMBER
	5e. TASK NUMBER
	5f. WORK UNIT NUMBER
7. PERFORMING ORGANIZATION NAME(S) AND ADDRESS(ES) **S-CUBED P. 0. Box 1620 La Jolla, CA 92038**	8. PERFORMING ORGANIZATION REPORT NUMBER
9. SPONSORING/MONITORING AGENCY NAME(S) AND ADDRESS(ES)	10. SPONSOR/MONITOR'S ACRONYM(S)
	11. SPONSOR/MONITOR'S REPORT NUMBER(S)

12. DISTRIBUTION/AVAILABILITY STATEMENT
Approved for public release, distribution unlimited

13. SUPPLEMENTARY NOTES
See also ADM002371. 2013 IEEE Pulsed Power Conference, Digest of Technical Papers 1976-2013, and Abstracts of the 2013 IEEE International Conference on Plasma Science. Held in San Francisco, CA on 16-21 June 2013. U.S. Government or Federal Purpose Rights License

14. ABSTRACT

15. SUBJECT TERMS

16. SECURITY CLASSIFICATION OF:			17. LIMITATION OF ABSTRACT	18. NUMBER OF PAGES	19a. NAME OF RESPONSIBLE PERSON
a. REPORT **unclassified**	b. ABSTRACT **unclassified**	c. THIS PAGE **unclassified**	**SAR**	**4**	

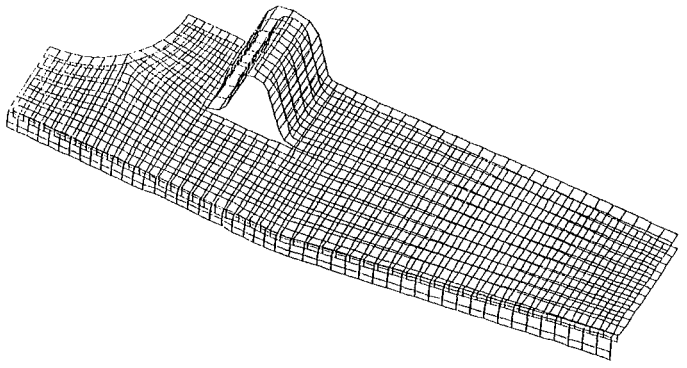

Figure 3. View of the computational mesh, representing half of the top side of one EAGLE module. Using mirror symmetry, this is sufficient to represent the full machine.

3. Calculations

Figure 3 shows a cut-away of the region of Double EAGLE which we treat - namely, the region extending from the pulse forming line (PFL) switch to the periphery of an annular resistive load. In the work presented here the voltage at the PFL switch is specified (Figure 4). For the purpose of this study - namely, to see what effect the TTE has on the propagation of the pulse, - this is adequate. The dimensions and pulse-shape correspond to specifications provided by Physics International.

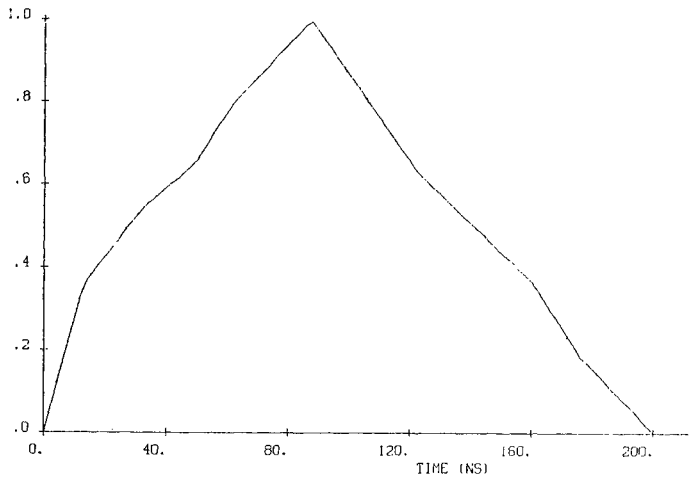

Figure 4. Assumed voltage at PFL input.

The inner and outer surfaces (cathode and anode) of the transmission line are treated as perfectly conducting and the water medium has a constant dielectric in which the signal velocity is

$$c \sim 3 \times 10^8 \varepsilon^{-1/2} \text{ m/s}$$

$$\sim 3.3 \times 10^7 \text{ m/s}$$

We assume that $\vec{A},\vec{E}$ have components only normal to the cathode-anode surfaces, and that mirror symmetry exists at all boundaries other than the PFL input (specified $\vec{E}$) and the load arc (matched impedance). This is exactly correct (assuming both modules and all switches operate in perfect synchrony) except for the physical edges of the TTE and side-rails, where it is a good approximation and corresponds to neglecting perturbation of power propagation by the fringing fields.

We now proceed to see what effect the TTE has on the propagation of the pulse by comparing results with those obtained in a geometry where the TTE is removed. Figures 5(a-h) show at four times (t = 99, 124, 149, and 223 ns) the voltage levels in the TTE and non-TTE geometries. The pulse arrives at the load (Figs. 5c,d) with a front which more closely matches the circular load in the TTE geometry than in the non-TTE case, so that vacuum region voltage (and power) gradients are initially much smaller in the TTE geometry. There is, however, a tendency for the wave to form itself to the load. At 149 ns (Figs. 5e,f) the flat geometry is slightly superior to the TTE. Figures 6 and 7 summarize the load voltage asymmetries. We see that during the initial voltage rise the TTE geometry does reduce considerably the angular variation of the voltage at the load. Subsequent "mode sloshing" results in alternately decreasing and increasing in the voltage variations in both geometries; however, the amplitude tends to be smaller in the TTE geometry.

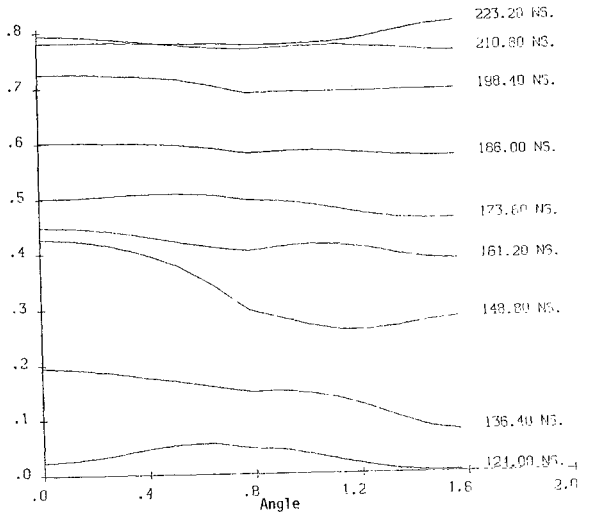

Figure 6. Voltage (TTE geometry) as a function of angle at the load arc for various times.

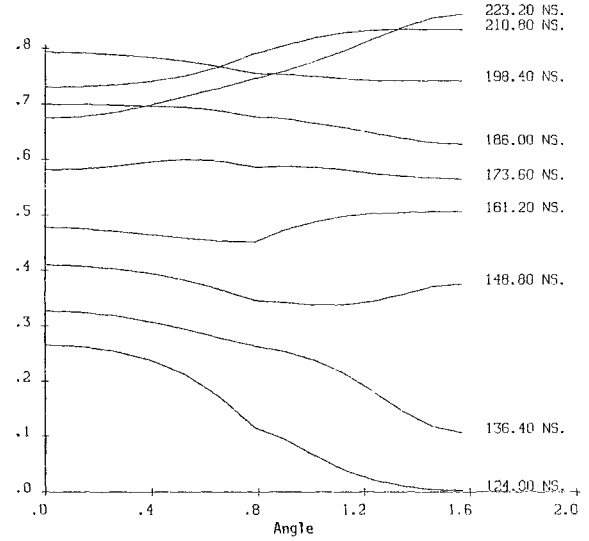

Figure 7. Voltage (flat geometry) as a function of angle at the load arc for various times.

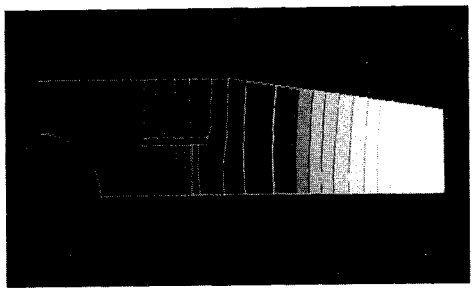

Figure 5a. Pulse in the TTE geometry at 99 ns. Peak of pulse is the second-rightmost contour band. Note delay at TTE.

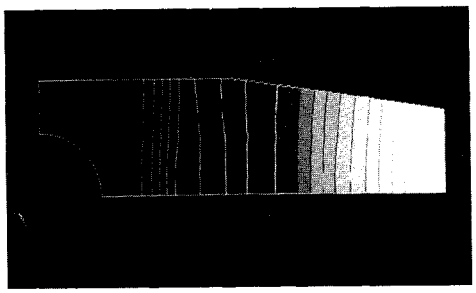

Figure 5b. Same as 5a in the flat geometry.

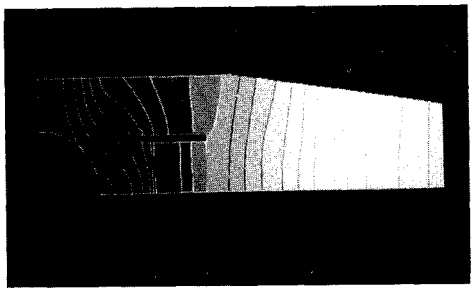

Figure 5c. Pulse in TTE geometry at 124 ns. Pulse is relatively uniformly incident on load at 45 .

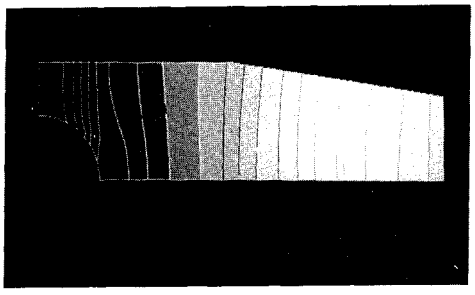

Figure 5d. Pulse in flat geometry at 124 ns. Substantial voltage gradients appear on load area.

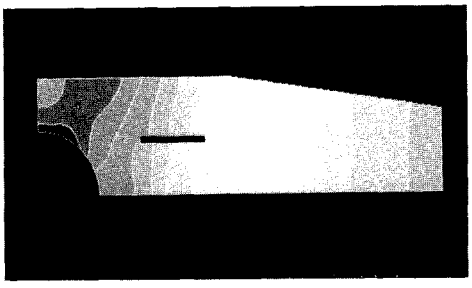

Figure 5e. Pulse in TTE geometry at 149 ns.

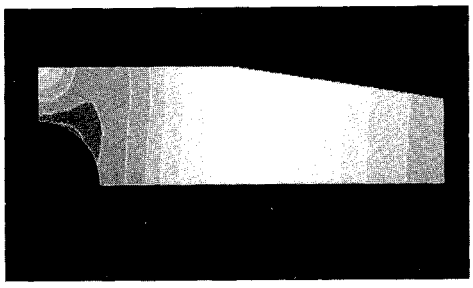

Figure 5f. Pulse in flat geometry at 149 ns. Flat is slightly superior to TTE at this time.

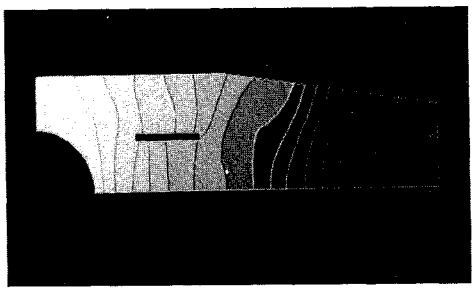

Figure 5g. Pulse in TTE at 223 ns, when the peak reaches the load.

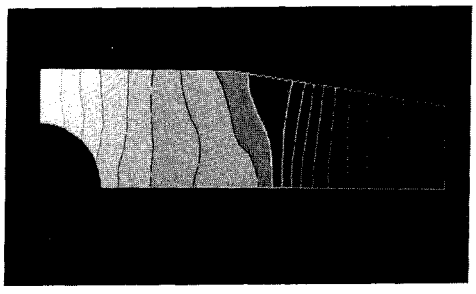

Figure 5h. Same as 5g for the flat geometry.

4. Conclusions

We have presented an electromagnetic model of the coupler region in Double EAGLE. The model is sufficiently general that it is applicable to arbitrary transmission line geometries in the long wavelength ($\lambda >> \Delta$) regime.

Based on the results obtained the Transit Time Equalizer proposed for use in Double EAGLE does reduce the asymmetry resulting from the geometry of the coupler regions.

References

1. Waisman, E. and A. Wilson, J.Appl. Physics 53, 731, (January 1982).
2. Frazier, G.B., "EAGLE and Double-EAGLE", (these proceedings).

Appendix

Finite Element Prescription for Laplacian Operator

Our treatment is based on the identity

$$d^3\underset{\sim}{r}\ \underset{\sim}{A}\cdot\nabla^2\underset{\sim}{A} + d^3\underset{\sim}{r}\ (\nabla\times\underset{\sim}{A})^2 = \text{surface terms}$$

Using finite element discretization, we may write the above as

$$V_i\ \underset{\sim}{A}_i\ \underset{\approx}{L}_{ij}\ \underset{\sim}{A}_u + \underset{\sim}{A}_i\ \underset{\approx}{M}_{ij}\ \underset{\sim}{A}_j = \text{surface terms},$$

where V_i is the volume associated with each node of the mesh. We then identify the Laplacian operator as

$$\underset{\approx}{L}_{ij} = V_i^{-1}\ \underset{\approx}{M}_{ij}$$

In our case, we have a quadrilateral mesh with the interelectrode spacing, D, and one component of $\underset{\sim}{A}$ defined at each node. The matrix M_{ij} is formed as the direct sum of contributions from each quadrilateral element as follows:

Define a transformation T between the quadrilateral and the unit square as

$$\underset{\sim}{r} = T(\mu,\nu) = (1-\mu)(1-\nu)\underset{\sim}{r}_1 + \mu(1-\nu)\underset{\sim}{r}_2 + \mu\nu\underset{\sim}{r}_3 + (1-\mu)\nu\ \underset{\sim}{r}_4$$

$$= \sum_{i=1}^{4} N_i(\mu,\nu)\underset{\sim}{r}_i$$

where $\underset{\sim}{r}_1 \ldots \underset{\sim}{r}_4$ are the actual coordinates of the corners of the quadrilateral. We interpolate

$$A(\mu,\nu) = \sum_{i=1}^{4} N_i(\mu,\nu)A_i$$

$$D(\mu,\nu) = \sum_{i=1}^{4} N_i(\mu,\nu)D_i$$

Since $\underset{\sim}{A}$ has only a normal component, A_n

$$\left|\nabla\times\underset{\sim}{A}\right|^2 = \left|\nabla A_n\right|^2 = \left|\sum_{i=1}^{4} A_i\nabla N_i\right|^2$$

and the contribution to M_{ij} from a given element is

$$M_{ij}^{(e)} = \int_0^1\int_0^1 \nabla N_i\cdot\nabla N_j\ D(\mu,\nu)\left|\frac{\partial\underset{\sim}{r}}{\partial\mu}\times\frac{\partial\underset{\sim}{r}}{\partial\mu}\right| d\mu d\nu\ .$$

To complete the prescription we find ∇N_i by solving the three equations

$$\frac{\partial\underset{\sim}{r}}{\partial\mu}\cdot\underset{\sim}{\nabla}N_i = \frac{\partial N_i}{\partial\mu}$$

$$\frac{\partial\underset{\sim}{r}}{\partial\nu}\cdot\underset{\sim}{\nabla}N_i = \frac{\partial N_i}{\partial\nu}$$

$$\hat{n}\cdot\underset{\sim}{\nabla}N_i = 0$$

where $\hat{n} = \frac{\partial\underset{\sim}{r}}{\partial\mu}\times\frac{\partial\underset{\sim}{r}}{\partial\nu}$. Also, the contribution of an element to a node volume is given by

$$V_i^{(e)} = \int_0^1\int_0^1 N_i\ D(\mu,\nu)\left|\frac{\partial\underset{\sim}{r}}{\partial\mu}\times\frac{\partial\underset{\sim}{r}}{\partial\nu}\right| d\mu\ d\nu\ .$$